AGU ADVANCING EARTH AND SPACE SCIENCE

Geophysical Research Letters

RESEARCH LETTER
10.1029/2020GL092087

Northeast Siberian Permafrost Ice-Wedge Stable Isotopes Depict Pronounced Last Glacial Maximum Winter Cooling

S. Wetterich[1], H. Meyer[1], M. Fritz[1], G. Mollenhauer[1], J. Rethemeyer[2], A. Kizyakov[3], L. Schirrmeister[1], and T. Opel[1]

[1]Alfred Wegener Institute Helmholtz Centre for Polar and Marine Research, Potsdam, Germany, [2]Institute of Geology and Mineralogy, University of Cologne, Cologne, Germany, [3]Department of Cryolithology and Glaciology, Faculty of Geography, Lomonosov Moscow State University, Moscow, Russia

Key Points:

- Pronounced west Beringian MIS 3 to MIS 2 winter cooling delineated in wedge-ice stable isotope signatures
- Coldest winters reflected by exceptionally depleted values of −37.4 ± 0.4‰ in $\delta^{18}O$ and −292 ± 3‰ in δD in LGM wedge ice
- LGM wedge ice directly radiocarbon-dated to 25,890 and 23,980 yr b2k

Supporting Information:

Supporting Information may be found in the online version of this article.

Correspondence to:

S. Wetterich,
sebastian.wetterich@awi.de

Citation:

Wetterich, S., Meyer, H., Fritz, M., Mollenhauer, G., Rethemeyer, J., Kizyakov, A., et al. (2021). Northeast Siberian permafrost ice-wedge stable isotopes depict pronounced last Glacial maximum winter cooling. *Geophysical Research Letters*, *48*, e2020GL092087. https://doi.org/10.1029/2020GL092087

Received 11 DEC 2020
Accepted 22 MAR 2021

Abstract Stable isotopes ($\delta^{18}O$, δD) of wedge ice hold potential to reconstruct past winter climate conditions. Here, we present records of the marine isotope stages (MIS) 3 and 2 including the last Glacial maximum (LGM) from Bol'shoy Lyakhovsky Island (NE Siberia). MIS 3 wedge ice dated from 52 to 40 Kyr b2k varies between −32 and −29‰ in $\delta^{18}O$. Colder LGM conditions are implied by $\delta^{18}O$ of −37‰ around 25 Kyr b2k. Similar Deuterium excess values indicate comparable moisture sources during MIS 3 and MIS 2. Regional LGM climate reconstructions depend on the seasonal resolution of the proxies and model simulations. Our wedge-ice record reflects coldest winters during global minima in atmospheric CO_2 and sea level. The extreme LGM winter cooling is not represented in model projections of global LGM climate where West Beringia shows noticeably little cooling or even warming in mean annual temperatures compared to the late Holocene.

Plain Language Summary The geochemical signature of stable isotopes of permafrost ground ice preserves information about past climate conditions. A common type of ground ice is ice wedges that form by the freezing of snowmelt in frost cracks developed on the ground and grow over time in width and length. Winter temperatures, and the type (snow or rain) and origin (regional moisture source) of winter precipitation largely control the stable isotope characteristics of oxygen and hydrogen in ice wedges. Here, we study the stable isotope composition of ice wedges from the last glacial period in northeastern Siberia. Plant and animal fossils that were found within the ice and in the surrounding frozen ground provide age control spanning from more than 50 to 24 thousand years ago when the ice wedges grew. The coldest winter conditions are inferred from a New Siberian Island ice-wedge site as indicated by the lowest stable isotope values of all our sampled ice wedges at times, corresponding to the last Glacial maximum around 25 thousand years ago.

1. Introduction

The last Glacial maximum (LGM), preceding the Deglacial and the Holocene, spans from 26.5 to 19 Kyr b2k (thousand years before the year 2000) on a global scale (Clark et al., 2009) during Marine Isotope Stage (MIS) 2. LGM characteristics include the maximum extent of Laurentide and Scandinavian ice sheets and global sea level minima (Lambeck et al., 2014). The unglaciated Arctic landmass and the exposed Bering Land Bridge formed Beringia—a vast space allowing for permafrost aggradation (Figure 1; Hopkins, 1959). Permafrost distribution and thickness reached their maxima during the LGM (Vandenberghe et al., 2014; Willeit & Ganopolski, 2015). Late Quaternary climate dynamics of consecutive stadial and interstadial periods were mainly driven by changes in radiative forcing as reflected in insolation curves (Laskar et al., 2004). The global climate oscillations are well represented in marine sediment (e.g., Lisiecki & Raymo, 2005) and ice cores (e.g., EPICA Community Members, 2004).

A modeling study by Tierney et al. (2020) combines sea-surface temperature data assimilation and an isotope-enabled climate model to investigate how the global climate system responds to changes in greenhouse gases and the cryosphere. Deduced annual mean surface air temperatures over land show LGM cooling of about −6°C on a global scale between 23 and 19 Kyr BP, but noticeably little cooling or even warming in West Beringia compared to the late Holocene. A similar pattern has been found for LGM summer

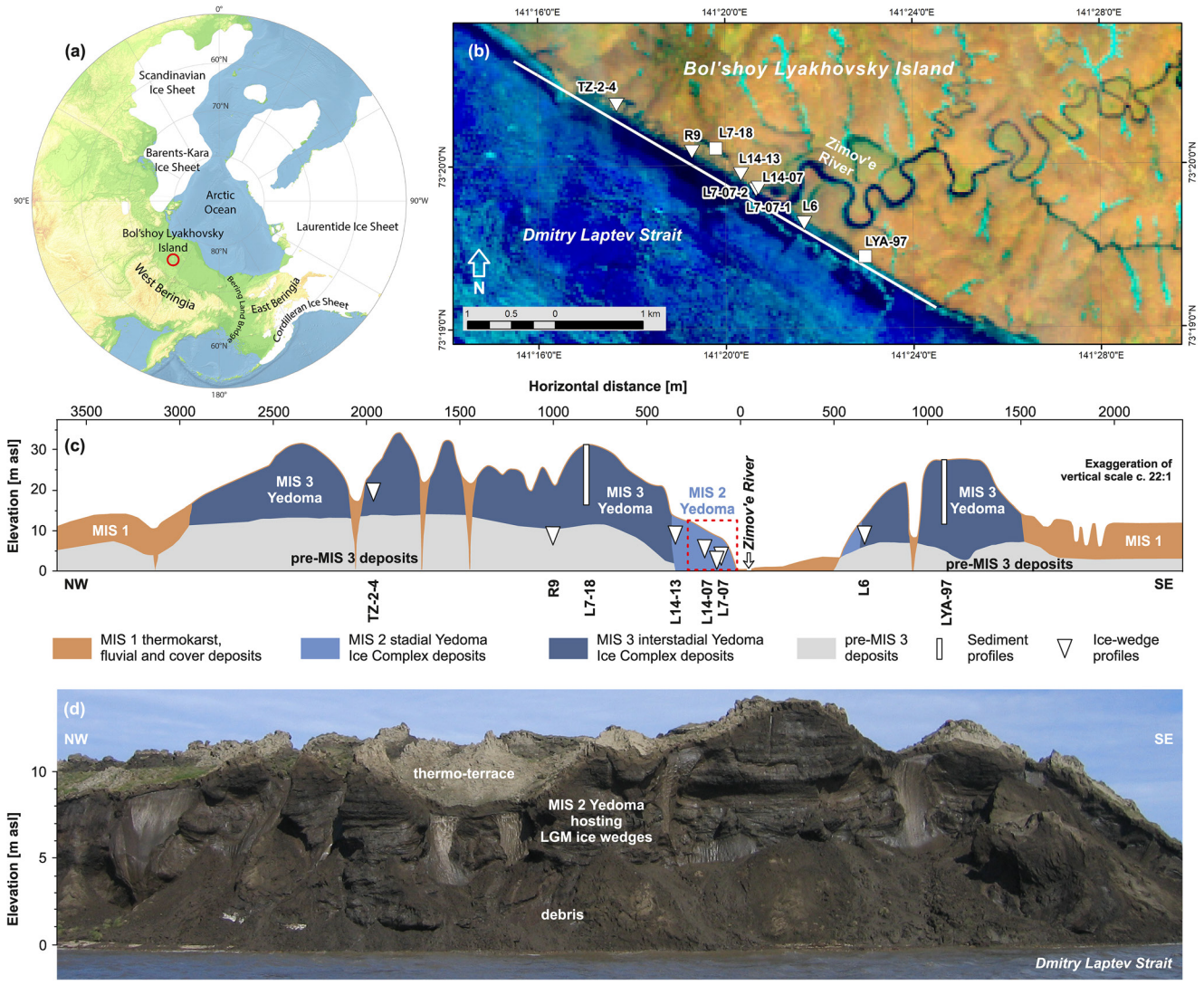

Figure 1. Study region and sampling locations in NE Siberia: (a) map with LGM ice sheets (Dyke et al., 2003; Manley & Kaufman, 2002; Svendsen et al., 2004), exposed shelf areas during LGM sea level lowstand of −120 m, and the position of Bol'shoy Lyakhovsky Island (red circle); (b) map of the study site (Landsat 5, June 27, 2009). The white line indicates the transect shown in (b); (c) coastal relief profile (after Andreev et al. (2009) with ice-wedge (triangles) and sediment (squares) profiles. (d) photograph of MIS 2 Yedoma Ice Complex hosting LGM ice wedges (dotted red rectangle in (c).

temperatures around 21 Kyr BP in West Beringia based on pollen records and modeling efforts (Weitzel et al., 2021). Similar-to-modern LGM summer temperatures between 20 and 18 Kyr BP have been reported by V. D. Meyer et al. (2017) on Kamchatka Peninsula in far-east Russia based on biomarker proxy data from marine sediments. LGM proxy records from West Beringia are generally sparse and have methodological limitations such as proxy uncertainties and seasonal biases which challenge the comprehensive understanding of LGM timing, magnitude, and spatial patterns on larger scales.

To reconstruct Beringian paleo-environments and climate such as those of the LGM, proxy data from permafrost deposits and ground ice are essential. Permafrost preserves both summer-specific fossils (Andreev et al., 2011; Kienast et al., 2011) and winter-specific wedge ice (e.g., Opel et al., 2018). The use of wedge ice stable oxygen ($\delta^{18}O$) and hydrogen (δD) isotopes as a winter temperature proxy arises from its distinct formation: Spring snowmelt fills polygonal winter thermal contraction cracks in the ground (i.e., ice-wedge polygons) and re-freezes, thus forming vertical ice veins (Leffingwell, 1915) that contain the isotopic composition of the winter time snowpack. By repeated frost cracking over long periods and with ongoing sedimentation, ice wedges grow syngenetically in width and height. Variations in stable water isotopes preserve

information on air temperature and moisture source for the cold season, that is the meteorological winter and spring (December to May, DJFMAM) as defined by H. Meyer et al. (2015).

To use ice wedges in paleoclimate research, chronologies are obtained from radiocarbon dating of fossil remains, CO_2, or dissolved organic carbon (DOC) preserved inside the wedge ice (e.g., Lachniet et al., 2012). Host sediments provide further indication of the ice-wedge formation age (Opel, Wetterich, et al., 2017). Dating of ice wedges can provide up to centennial resolution as shown for the Younger Dryas (H. Meyer et al., 2010). Stacked records of dated Holocene stable isotope samples combined from multiple sites (Holland et al., 2020; H. Meyer et al., 2015) or from a single site (Opel, Laepple, et al., 2017) represent state-of-the-art approaches to deduce reliable ice-wedge chronologies. However, wedge-ice chronologies from the late Pleistocene are less constrained (H. Meyer, Dereviagin, Siegert, & Hubberten, 2002; Opel, Wetterich, et al., 2017, Opel et al., 2019) and scarce (Porter & Opel, 2020), but crucial for a better regional and seasonal assessment of LGM climate.

Here, we present radiocarbon ages and stable isotope data of ice wedges from Yedoma Ice Complex of MIS 3-2 age exposed at the southern coast of Bol'shoy Lyakhovsky Island (New Siberian Archipelago) (Figure 1). Specifically, we seek (1) to quantify isotopic changes in glacial winter climate conditions from interstadial MIS 3 to stadial MIS 2, (2) to constrain the timing of the coldest winter conditions during the LGM, and (3) to present new insights into LGM cooling and regional seasonality patterns in Beringia.

2. Material and Methods

2.1. Ice-Wedge Sampling

Bol'shoy Lyakhovsky is the southernmost island of the New Siberian Archipelago at the Dmitry Laptev Strait and located in West Beringia (Figure 1a). The southern coast near the Zimov'e River mouth exposes late Quaternary permafrost and has been intensively studied in recent decades (e.g., Schirrmeister et al., 2011; Tumskoy et al., 2012).

The Bol'shoy Lyakhovsky permafrost sequences exposed in coastal bluffs discontinuously cover approximately the last 200 Kyr (Schirrmeister et al., 2002; Wetterich et al., 2019). Four distinct Ice Complex generations of MIS 7, MIS 5, MIS 3, and MIS 2 age are exposed, intersected by floodplain deposits of MIS 6 and MIS 4 age as well as by MIS 5 thermokarst deposits, and covered by Holocene deposits (Andreev et al., 2011; Wetterich et al., 2009, 2016, 2019). Substantial parts of the exposed permafrost belong to the Yedoma Ice Complex of MIS 3-2 age (H. Meyer, Dereviagin, Siegert, Schirrmeister, et al., 2002; Wetterich et al., 2011, 2014), which is the focus of this study. Modern wedge-ice growth takes preferentially place in thermokarst basins and on the Zimov'e river floodplain.

In total, seven ice wedge profiles from MIS 3-2 Yedoma Ice Complex are considered in our study (Figures 1b and 1c). The profiles exposed over a total distance of about 2.5 km were sampled in 1999, 2007, and 2014 either by ice screw or by chainsaw. More details are given in the supporting information S1.

2.2. Radiocarbon Dating

The radiocarbon dating of organic material from host deposits and wedge-ice inclusions was performed at CologneAMS (University of Cologne, Germany; Rethemeyer et al., 2019), at Leibniz Laboratory for Radiometric Dating and Stable Isotope Research (Kiel, Germany; Grootes et al., 2004) and at MICADAS (Mini Carbon Dating System, AWI, Bremerhaven, Germany; Opel et al., 2019). In total, eight new radiocarbon dates from distinct floral or faunal macrofossils (>1 mm in size) and seven re-calibrated dates from H. Meyer, Dereviagin, Siegert, Schirrmeister, et al. (2002) and Wetterich et al. (2011) are considered (Table S1). Ages are given as median values of calibrated years before the year 2000 (yr b2k) using the IntCal20 calibration data set (Reimer et al., 2020).

2.3. Ice-Wedge Stable Isotopes

Melted ice samples were analyzed for oxygen ($\delta^{18}O$) and hydrogen (δD) stable isotopes using a Finnigan MAT Delta-S mass spectrometer ($1\sigma < 0.1‰$ for $\delta^{18}O$, $1\sigma < 0.8‰$ for δD; H. Meyer et al., 2000). The values

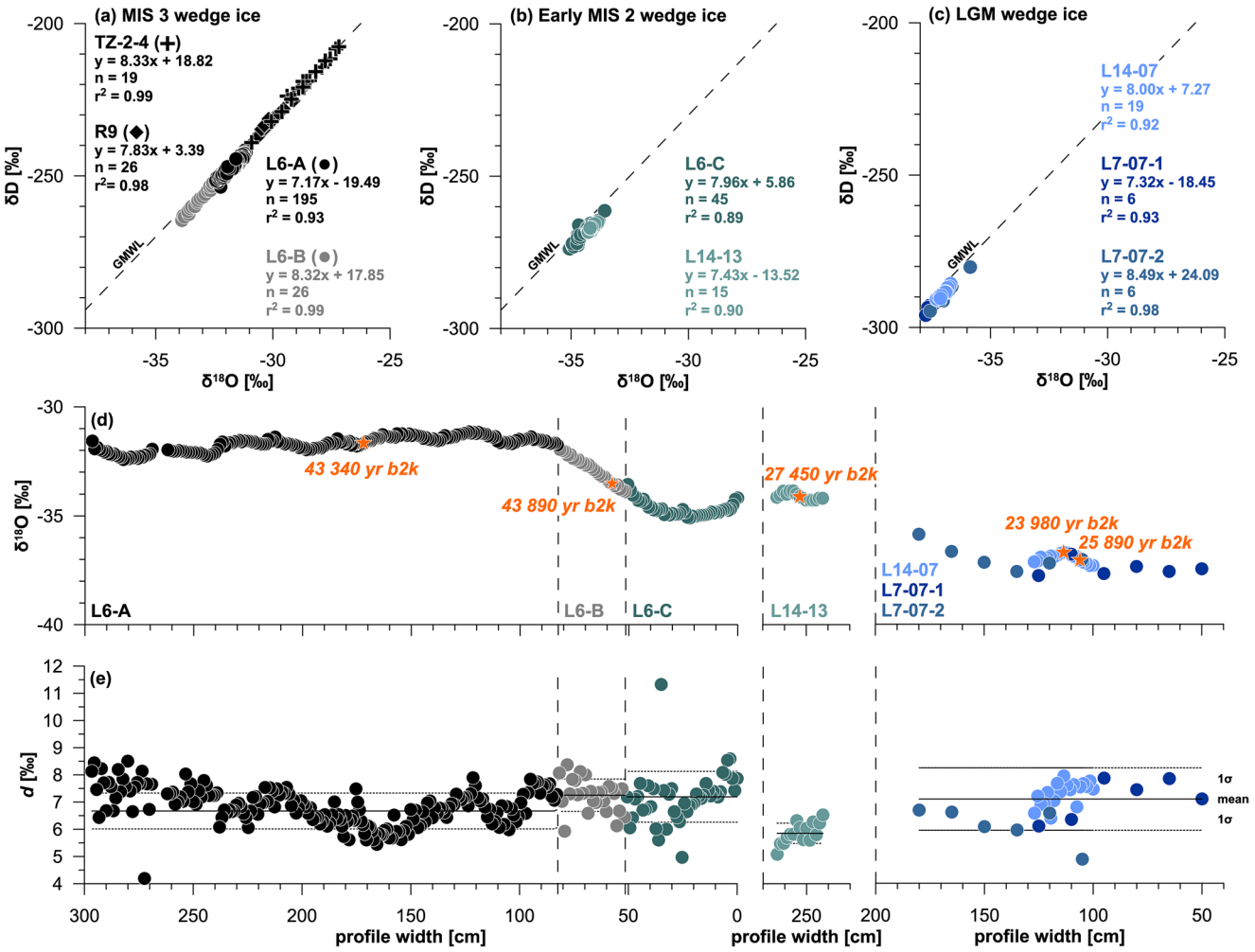

Figure 2. Stable water isotope composition ($\delta^{18}O$, δD) of (a) Yedoma ice wedges of MIS 3 (black symbols), (b) early MIS 2 (greenish symbols), and (c) LGM (bluish symbols) ages. Directly dated wedge-ice R9 (black diamonds) and TZ-2-4 (black crosses; H. Meyer, Dereviagin, Siegert, Schirrmeister, et al., 2002) are shown for comparison in (a). L7-07 data shown in (c) are from Wetterich et al. (2011). Radiocarbon-dated ice wedge profiles of (d) $\delta^{18}O$ and (e) deuterium excess (d) delineating the MIS 3 to MIS 2 transition toward LGM are shown. Orange asterisks in (d) indicate the dated samples. Profile means and 1σ rages in (e) are indicated by lines and dotted lines, respectively. Note that data from L14-13 and from L14-07 derive from ice wedges that were sampled only in their central parts.

are reported as per mil (‰) difference from the VSMOW (Vienna Standard Mean Ocean Water). The deuterium excess (d) is calculated according to Dansgaard (1964) in Equation 1:

$$d = \delta D - 8 * \delta^{18}O \quad (1)$$

In total, 357 samples from seven ice wedges were analyzed (Table S2; Figure 2). The study focuses on $\delta^{18}O$ as it is more commonly used in Arctic ground ice paleoclimate studies. Respective δD values are given in Table S2.

3. Results and Discussion

3.1. Ice-Wedge Formation Ages

The formation of the MIS 3 Yedoma Ice Complex of Bol'shoy Lyakhovsky is constrained by numerous radiocarbon dates from frozen deposits. Two 15-m-thick vertical sequences reflect continuous Yedoma formation between >50 and 32.7 Kyr b2k (LYA-97; Andreev et al., 2009) and between >50 and 33.4 Kyr b2k (L7–18; Wetterich et al., 2014), highlighting the quasi-symmetric distribution of stratigraphic sequences in

similar geomorphologic positions west and east of the Zimov'e River (Figure 1c). Scarce radiocarbon ages from MIS 3 Yedoma wedge ice range from 51.7 to 39.5 Kyr b2k (H. Meyer, Dereviagin, Siegert, Schirrmeister, et al., 2002). Newly obtained dates from woody inclusions in the older part of ice wedge L6 fit into that range (43.3 Kyr b2k in L6-A and 43.9 Kyr b2k in L6-B) (Table S1).

Evidence of continued Ice Complex accumulation during MIS 2 on Bol'shoy Lyakhovsky was only found in slope positions of the Zimov'e River valley, but not on top of nearby MIS 3 Ice Complex (Figure 1c). This change in accumulation area can be explained by a lowered erosion base during LGM sea level lowstand and corresponding changes in the hydrological system of areas with higher relief inclination leading to preferential Ice Complex formation in valley areas (Wetterich et al., 2011). On the Zimov'e River valley slope, previously published radiocarbon dates (Wetterich et al., 2011) and new data from in situ *Rangifer tarandus* bones confirm MIS 2 Yedoma Ice Complex formation from about 30 to 26 Kyr b2k. However, one age of 34 Kyr b2k (*Equus* sp.) bone is interpreted as re-deposited, possibly by downslope slumping from above-lying MIS 3 deposits (Table S1). New dates from MIS 2 Yedoma ice wedges show ages of 27.5 Kyr b2k (L14-13), 25.9 and 24 Kyr b2k (both L14-07; Table S1). Thus, the overall MIS 2 Ice Complex formation spans from 30 to at least 24 Kyr b2k.

Syngenetic wedge ice is younger than the host deposits at the same elevation level due to the ice-wedge formation in vertical frost cracks within older sediments (Porter & Opel, 2020). Such age offset is systematic and defined by the cracking depth and permafrost aggradation rates. In the MIS 2 Yedoma record of Bol'shoy Lyakhovsky Island, three in situ *R. tarandus* bones sampled at 7 masl range between 26.2 and 26 Kyr b2k, while the dates of ice wedge L14-07 at the same sampling height are slightly younger with 25.9 Kyr b2k and 24 Kyr b2k (Table S2). The corresponding ages of MIS 2 host deposits and wedge ice suggest reliable age information.

3.2. Stable Isotope Composition of Wedge Ice

Yedoma wedge ice of MIS 3 and MIS 2 age from Bol'shoy Lyakhovsky has distinct stable isotope compositions (Table S2). MIS 3 ice wedge $\delta^{18}O$ mean values vary between $-32.0 \pm 0.3‰$ and $-28.7 \pm 0.9‰$ (Figure 2a). Early MIS 2 wedge ice shows more depleted $\delta^{18}O$ mean values between $-34.7 \pm 0.4‰$ and -34.1 ± 0.2 (Figure 2b), while the most depleted $\delta^{18}O$ mean values are seen in LGM ice between $-37.4 \pm 0.4‰$ and $-37.0 \pm 0.2‰$ (Figure 2c).

The MIS 3 Yedoma ice wedges show more depleted mean $\delta^{18}O$ values in the 51.7 Kyr b2k old ice of R9 ($-30.1 \pm 0.4‰$) and the 43.3 Kyr b2k old ice of L6-A ($-32.0 \pm 0.3‰$) if compared to the 39.5 Kyr b2k old ice of TZ-2-4 ($-28.7 \pm 0.9‰$; Figure 2a). Post-depositional isotopic exchange processes within the ice probably smoothed the original isotopic composition to some degree although the distinct signatures are still seen. The mean *d* in MIS 3 wedge ice varies between 6.8 and 9.3‰ and the slopes in $\delta^{18}O$-δD linear regressions range from 7.2 to 8.3 (Figure 2a).

Within ice wedge profile L6 a smooth and directed transition from MIS 3 ice of L6-A ($\delta^{18}O$ of $-32.0 \pm 0.3‰$) toward more depleted isotopic values of L6-C ($\delta^{18}O$ of $-34.7 \pm 0.4‰$) is obvious, and differentiated as L6-B ($\delta^{18}O$ of $-32.9 \pm 0.6‰$ in) with decreasing $\delta^{18}O$ toward the ice-wedge margin (Figure 2d). Given the overlapping 1σ age ranges of L6-A (42.5–44.1 Kyr b2k) and L6-B (42.6–44.8 Kyr b2k), we hypothesize a change in the prevailing frost cracking dynamics possibly due to a change in the polygonal pattern, and, hence, rather lateral growth for ice wedge L6, although the L6-C part has not been dated. We regard the L6-B age as derived from re-deposited organic material, and consequently omit it from interpretation. Irregular growth differing from the central ice-wedge growth model (Lachenbruch, 1962) has been previously reported (Lachniet et al., 2012; Mackay & Burn, 2002; Opel et al., 2011), and is thought to explain the directed isotopic trend from L6-A to L6-C by a presumably lateral growth direction. The addition of younger ice laterally (L6-C) is also supported by field observations (Figure S3). The L6-C wedge ice is isotopically very close to the L14-13 wedge ice record (27.5 Kyr b2k; $\delta^{18}O$ of $-34.1 \pm 0.2‰$, *d* of $5.9 \pm 0.4‰$; Table S2) although the mean *d* value in L6-C ($7.2 \pm 0.9‰$) is slightly higher (Figure 2e). Both ice wedges, L14-13 and L6-C were sampled in similar stratigraphic and morphologic positions west and east of the Zimov'e River mouth, respectively (Figure 1c). Thus, given the very similar isotopic composition, we assume a formation time for both ice wedges L14-13 and L6-C during the early MIS 2 reflecting a winter cooling trend.

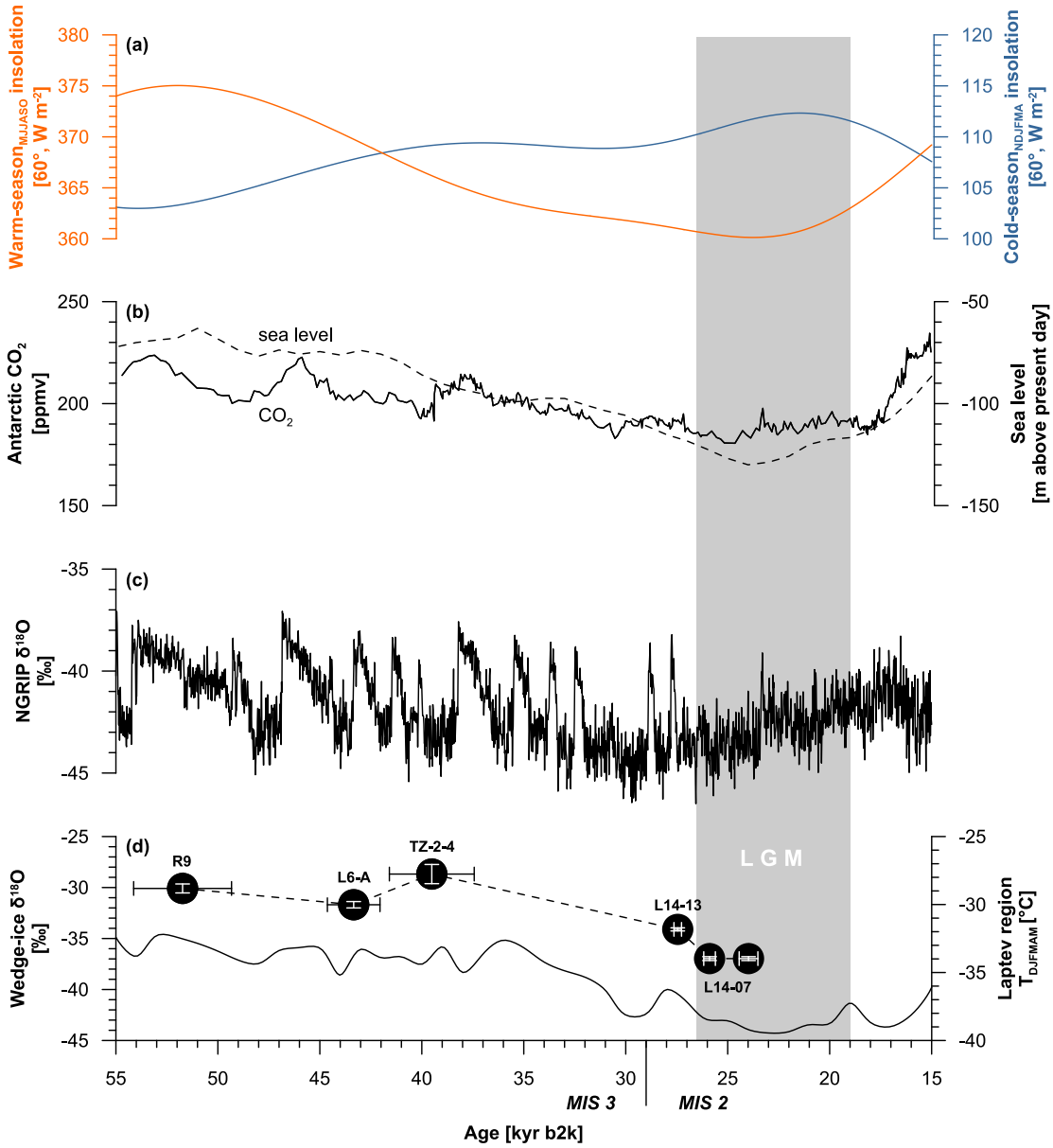

Figure 3. MIS 3 to MIS 2 climate forcing and variability: (a) seasonal insolation of the winter (NDJFMA) and summer (MJJASO) seasons at 60°N (Laskar et al., 2004); (b) CO_2 concentration derived from Antarctic ice cores (solid line; Lüthi et al., 2008) and global sea level (dotted line; Spratt & Lisiecki, 2016); (c) NGRIP $\delta^{18}O$ (NGRIP Members, 2004), and (d) Mean $\delta^{18}O$ values (and standard deviations) of directly radiocarbon-dated ice wedge profiles (Table S1) on Bol'shoy Lyakhovsky Island shown together with modeled cold-season surface temperatures of the Laptev Sea region (DJFMAM, Ganopolski & Calov, 2011). The LGM period is shown as gray-shaded area.

LGM wedge ice was encountered in ice wedge profile L14-07 (25.9 and 24 Kyr b2k) as well as in ice wedges L7-07-1 and L7-07-2 of the same isotopic composition (Figure 2c). These records represent LGM winter conditions with most depleted mean $\delta^{18}O$ values of up to -37.4 ± 0.4‰ and mean *d* between 6.1 and 7.3‰ (Table S2).

3.3. Paleoclimatic Implications of Wedge-Ice $\delta^{18}O$ and Deuterium Excess

The variations in ice wedge stable isotopes from Bol'shoy Lyakhovsky correspond to large-scale interstadial MIS 3 and stadial MIS 2 climate conditions, including the LGM (Figure 3). The coldest winters are reflected by the most depleted $\delta^{18}O$ and δD values in LGM ice around 25 Kyr b2k. Less depleted MIS 3 stable isotopes

imply relatively higher winter temperatures and indicate more variable interstadial conditions between >51.7 and 39.5 Kyr b2k.

The deuterium excess in wedge ice is influenced by local conditions (Opel et al., 2018) as well as by isotopic smoothing with time, but is commonly applied to deduce changes in moisture generation and transport. Thus, ice wedge *d* might serve as a potential indicator of shifting moisture sources related to changing major atmospheric circulation patterns (H. Meyer et al., 2010) or sea ice cover. The mean *d* values in MIS 3-2 wedge ice overlap. The MIS 3 mean values of *d* vary only between 6.8 ± 0.7‰ and 9.3 ± 0.9‰ and those for MIS 2 even less between 5.9 ± 0.4 ‰ and 7.3 ± 0.4‰ (Table S2). We therefore infer that winter moisture sources for Bol'shoy Lyakhovsky Island remained relatively stable during MIS 3-2. Consequently, variations in MIS 3-2 wedge-ice $\delta^{18}O$ are thought to reflect winter temperature changes. We assume the North Atlantic and potentially the North Pacific as main moisture sources with varying contributions to the precipitation eventually forming the ice wedges. To which extent both moisture sources finally contributed to winter precipitation of our study region during MIS 3-2 is yet unknown. Further, minor contributions of proximal primary and secondary sources are possible but unlikely due to the persistent sea ice cover and frozen open water bodies in the winter season.

The interstadial MIS 3 wedge ice of Bol'shoy Lyakhovsky varies over about 3‰ in $\delta^{18}O$, which is less than half the amplitude seen in the NGRIP ice core for the same time slice that is driven by prominent Dansgaard-Oeschger (D-O) events: rapid climate oscillations that originated in the North Atlantic region (Figure 3c; Dansgaard et al., 1993). Those are not identified but only hypothesized in Siberian climate archives yet (Baumer et al., 2021). The temporal resolution of ice wedge stable isotope records would not allow recognizing D-O events yet even though they might have impacted East Siberian climate dynamics. The different range in MIS 3 isotopes might also relate to the differences in seasonality represented in the two archives and spatial coverage. Bol'shoy Lyakhovsky wedge ice reflects regional winter temperatures while the Greenlandic ice rather represents the North Atlantic annual temperatures and does not specifically resolve the winter-season. The NGRIP LGM signal is not characterized by most depleted isotope values, but varies within its MIS 3 range. In contrast, Bol'shoy Lyakhovsky LGM wedge ice $\delta^{18}O$ values are up to 9‰ lower than MIS 3 maxima (Figure 3d).

To estimate the LGM cooling in relation to the interglacial MIS 1, Holocene and modern wedge ice has to be considered. On Bol'shoy Lyakhovsky, early to mid-Holocene thermokarst deposits dated from 8400 to 4460 yr b2k contain wedge ice with −23.6 ± 1.4‰ in $\delta^{18}O$ (Wetterich et al., 2009). At the same place, late Holocene ice wedges dated to 790 and 170 yr b2k exhibit $\delta^{18}O$ of −24.6 ± 1.3‰ and −24.4 ± 0.8‰, respectively (H. Meyer, Dereviagin, Siegert, Schirrmeister, et al., 2002). Modern ice wedges representing the last ~30 years before sampling in 1999 show even less depleted $\delta^{18}O$ (−20.4 ± 1.3‰; H. Meyer, Dereviagin, Siegert, Schirrmeister, et al., 2002). Thus, the LGM winter cooling is expressed by up to 13 ‰ more depleted $\delta^{18}O$ compared to Holocene records and by up to 17‰ more depleted $\delta^{18}O$ compared to modern wedge ice.

In general, distinct LGM wedge-ice records showing extremely cold winter conditions are rare on the circum-arctic scale (Porter & Opel, 2020). In eastern Beringia, Lachniet et al. (2012) found a 6‰ decrease in $\delta^{18}O$ within one ice wedge that formed between 28 and 22 Kyr b2k, reflecting LGM cooling. More often, similar MIS 3 and MIS 2 isotopic signatures are found (Porter & Opel, 2020). Indirectly dated MIS 2 wedge ice (28.4 Kyr b2k) on Bykovsky Peninsula (Laptev Sea) shows $\delta^{18}O$ of −30.8 ± 0.6‰; well within the range of MIS 3 ice wedge isotopic compositions at this location (H. Meyer, Dereviagin, Siegert, & Hubberten, 2002). MIS 2 wedge-ice, directly dated to 25.3 and 23.5 Kyr b2k, from Sobo-Sise Island (Lena Delta) with mean $\delta^{18}O$ of −28.8 ± 0.5‰ does not differ much from MIS 3 ($\delta^{18}O$ from −31.4 ± 1.1 to −30.5 ± 0.8‰; Wetterich et al., 2020). Hitherto, it is not sufficiently resolved yet, whether this is due to a less cold LGM climate in the region or poor LGM representation in the studied ice wedge profiles. Therefore, the well-dated Bol'shoy Lyakhovsky LGM wedge-ice record is exceptional and requires further explanation.

Porter and Opel (2020) emphasize that rare LGM wedge-ice records might be explained by local winter conditions affecting ice-wedge formation when thick snow cover potentially prevented frost cracking. Alternatively, thin or no snow cover and deflation at exposed terrain surfaces by enhanced winter storm activity (Guthrie, 2001) might not have provided sufficient melt water for wedge-ice formation during the LGM. For our record, we consider that the slope position of MIS 2 Yedoma Ice Complex may have promoted

accumulation of snow drift potentially leading to an overrepresentation of isotopically more depleted precipitation from the coldest period of the winter time that became preserved in the LGM wedge ice. If so, during MIS 3 and MIS 2 the local conditions of Ice Complex formation differed considerably and could therefore have superimposed the general interstadial-stadial winter climate pattern.

However, both the interstadial and the stadial climate patterns as reflected in our wedge-ice records are supported by variations in global atmospheric CO_2 concentrations (Lüthi et al., 2008) and in sea level reconstructions (Spratt & Lisiecki, 2016) (Figure 3). The Bol'shoy Lyakhovsky ice-wedge record is further in line with modeled cold-season air temperatures of the Laptev Sea region (Ganopolski & Calov, 2011). This model output is based on an Earth system model of intermediate complexity, mainly forced by Earth's orbital parameters and atmospheric concentration of major greenhouse gases (Ganopolski & Calov, 2011; Petoukhov et al., 2000). Although a calibrated relationship between wedge-ice $\delta^{18}O$ and cold-season air temperature has not been developed yet for northern Eurasia (Opel et al., 2018), the isotopic depletion of 9‰ in $\delta^{18}O$ between warmest interstadial MIS 3 and coldest stadial MIS 2 periods would correspond to modeled cold-season LGM temperatures up to 6°C lower than during MIS 3 (Figure 3) if temperature alone controlled the wedge-ice $\delta^{18}O$.

Holocene ice-wedge records show increasing $\delta^{18}O$ corresponding to the mid to late Holocene winter warming that is related to increasing cold-season insolation and partially by rising greenhouse gas concentrations (Holland et al., 2020; H. Meyer et al., 2015; Opel, Laepple, et al., 2017). In contrast, the LGM winter cooling appears not to be controlled by cold-season insolation, which increased over this period (Figure 3). Instead, the overall LGM cooling was driven by a strong minimum in summer and annual insolation in mid to high northern latitudes due to orbital cycles (Milankovitch, 1941). Between about 53 and 22 Kyr b2k, the decrease in summer insolation of about 15 W m^{-2} dominated over the winter insolation increase of about 9 W m^{-2} (Figure 3) leading finally to overall full glacial conditions of the LGM. Less pronounced orbitally driven seasonality during MIS 2 would imply smaller temperature amplitudes between LGM summers and winters in contrast to higher seasonality with higher seasonal temperature amplitudes during MIS 3. However, this potential effect seems superimposed by increased continentality with a stronger Siberian High and stronger winter cooling for MIS 2 in the study region as a result of the northern hemispheric configuration of ice sheets, sea ice coverage on the Arctic Ocean and global sea level lowstand (Guthrie, 2001; Murton et al., 2015).

The substantial LGM winter cooling under highly continental conditions as reflected in the Bol'shoy Lyakhovsky ice-wedge stable isotope record complements the results of recent LGM climate modeling studies. Modeled annual LGM temperatures (Tierney et al., 2020) and summer-season LGM temperatures (Weitzel et al., 2021) as well as biomarker-based summer-season temperature reconstructions (V. D. Meyer et al., 2017) indicate only slightly colder or even warmer LGM conditions than today in East Siberia (West Beringia) for periods slightly post-dating the present winter-season record. By highlighting the seasonal biases of the different studies, the apparent differences imply the need for well-dated regionally constrained seasonal-scale temperature reconstructions and climate model output for holistically assessing the climate conditions of particular time periods such as the LGM.

4. Conclusions

Directly dated ice wedges are the only conclusive winter climate archives for the late Pleistocene in Beringia. However, winter climate variability between interstadial MIS 3 and stadial MIS 2, including the last Glacial maximum, has not yet been well constrained by radiocarbon-dated ice wedge stable isotope records. One exception from West Beringia is found on Bol'shoy Lyakhovsky Island. Here, interstadial MIS 3 winter climate variability is reflected by mean $\delta^{18}O$ values between −32 and −29‰ (dated to 51.7 to 39.5 Kyr b2k) followed by early MIS 2 cooling reflected by mean $\delta^{18}O$ values from −35 to −34‰ (dated to 27.5 Kyr b2k) and the full LGM with −37‰ in $\delta^{18}O$ (dated to 25.9 to 24 Kyr b2k). However, as chronologically less constrained records further west in the Central Laptev Sea coastal region do not show this prominent LGM winter temperature minimum, and local conditions in snow distribution and consecutive wedge-ice formation might have affected the finally preserved isotopic signal in addition to climate.

Increased continentality in the study region was caused by the LGM sea level minimum. Together with the northern hemispheric configuration of ice sheets and a persistent Arctic Ocean sea ice cover in winter, a stronger Siberian High and thus stronger winter cooling are likely. The Bol'shoy Lyakhovsky LGM ice-wedge record reflects coldest winter conditions in NE Siberia during global minima in atmospheric CO_2 and sea level. Cool and dry LGM summers as deduced from biological proxy data and exceptionally cold LGM winters as seen in the present study correspond to low seasonality with smaller seasonal temperature amplitudes compared to MIS 3.

Conflict of Interest

The authors declare no conflicts of interest relevant to this study.

Data Availability Statement

The ice wedge stable isotope and radiocarbon data are available at https://doi.pangaea.de/10.1594/PANGAEA.927621 (Wetterich et al., 2021).

Acknowledgments
We thank the LENA expedition for logistic support and our colleagues working with us in the field in 1999, 2007, and 2014. Laboratory work was supported by Mikaela Weiner, Lutz Schönicke (Stable Isotope Facility at AWI Potsdam) as well as by Elizabeth Bonk and Torben Gentz (MICADAS at AWI Bremerhaven). We thank Editor Valerie Trouet and two anonymous reviewers as well as Go Iwahana for their feedback that led to an improved paper. Funding was provided by Deutsche Forschungsgemeinschaft (DFG grant no. WE4390/7-1 to S. Wetterich) and the German Federal Ministry of Education and Research (CARBOPERM Project, BMBF grant no. 03G0836A).

References

Andreev, A. A., Grosse, G., Schirrmeister, L., Kuznetsova, T. V., Kuzmina, S. A., Bobrov, A. A., et al. (2009). Weichselian and Holocene palaeoenvironmental history of the Bol'shoy Lyakhovsky Island, New Siberian Archipelago, Arctic Siberia. *Boreas*, *38*, 72–110. https://doi.org/10.1111/j.1502-3885.2008.00039.x

Andreev, A. A., Schirrmeister, L., Tarasov, P. E., Ganopolski, A., Brovkin, V., Siegert, C., et al. (2011). Vegetation and climate history in the Laptev Sea region (Arctic Siberia) during Late Quaternary inferred from poll records. *Quaternary Science Reviews*, *30*, 2182–2199. https://doi.org/10.1016/j.quascirev.2010.12.026

Baumer, M. M., Wagner, B., Meyer, H., Leicher, N., Lenz, M., Fedorov, G., et al. (2021). Climatic and environmental changes in the Yana Highlands of north-eastern Siberia over the last c. 57 000 years, derived from a sediment core from Lake Emanda. *Boreas*, *50*, 114–133. https://doi.org/10.1111/bor.12476

Clark, P. U., Dyke, A. S., Shakun, J. D., Carlson, A. E., Clark, J., Wohlfarth, B., et al. (2009). The last glacial maximum. *Science*, *325*(5941), 710–714. https://doi.org/10.1126/science.1172873

Dansgaard, W. (1964). Stable isotopes in precipitation. *Tellus*, *16*(4), 436–468. https://doi.org/10.3402/tellusa.v16i4.8993

Dansgaard, W., Johnsen, S. J., Clausen, H. B., Dahl-Jensen, D., Gundestrup, N. S., Hammer, C. U., et al. (1993). Evidence for general instability of past climate from a 250-kyr ice-core record. *Nature*, *364*, 218–220. https://doi.org/10.1038/364218a0

Dyke, A. S., Moore, A., & Robertson, L. (2003). *Deglaciation of North America*. Geological Survey of Canada Open File, 1574. Thirty-two digital maps at 1:7,000,000 scale with accompanying digital chronological database and one poster (two sheets) with full map series.

EPICA Community Members. (2004). Eight glacial cycles from an Antarctic ice core. *Nature*, *429*, 623–628. https://doi.org/10.1038/nature02599

Ganopolski, A., & Calov, R. (2011). The role of orbital forcing, carbon dioxide and regolith in 100 kyr glacial cycles. *Climate of the Past*, *7*, 1415–1425. https://doi.org/10.5194/cp-7-1415-2011

Grootes, P. M., Nadeau, M.-J., & Rieck, A. (2004). ^{14}C-AMS at the Leibniz-Labor: Radiometric dating and isotope research. *Nuclear Instruments and Methods in Physics Research Section B*, *223–224*, 55–61. https://doi.org/10.1016/j.nimb.2004.04.015

Guthrie, R. D. (2001). Origin and causes of the mammoth steppe: A story of cloud cover, woolly mammal tooth pits, buckles, and inside-out Beringia. *Quaternary Science Reviews*, *20*, 549–574. https://doi.org/10.1016/S0277-3791(00)00099-8

Holland, K. M., Porter, T. J., Froese, D. G., Kokelj, S. V., & Buchanan, C. A. (2020). Ice-wedge evidence of Holocene winter warming in the Canadian Arctic. *Geophysical Research Letters*, *47*, e2020GL087942. https://doi.org/10.1029/2020gl087942

Hopkins, D. M. (1959). Cenozoic history of the Bering Land Bridge: The seaway between the Pacific and Arctic basins has often been a land route between Siberia and Alaska. *Science*, *129*(3362), 1519–1528. https://doi.org/10.1126/science.129.3362.1519

Kienast, F., Wetterich, S., Kuzmina, S., Schirrmeister, L., Andreev, A. A., Tarasov, P., et al. (2011). Paleontological records indicate the occurrence of open woodlands in a dry inland climate at the present-day Arctic coast in western Beringia during the last interglacial. *Quaternary Science Reviews*, *30*(17–18), 2134–2159. https://doi.org/10.1016/j.quascirev.2010.11.024

Lachenbruch, A. H. (1962). Mechanics of thermal contraction cracks and ice-wedge polygons in permafrost. *Geological Society of America Special Papers*, *70*, 1–66. https://doi.org/10.1130/spe70-p1

Lachniet, M. S., Lawson, D. E., & Sloat, A. R. (2012). Revised C-14 dating of ice wedge growth in interior Alaska (USA) to MIS 2 reveals cold paleoclimate and carbon recycling in ancient permafrost terrain. *Quaternary Research*, *78*, 217–225. https://doi.org/10.1016/j.yqres.2012.05.007

Lambeck, K., Rouby, H., Purcell, A., Sun, Y., & Sambridge, M. (2014). Sea level and global ice volumes from the Last Glacial Maximum to the Holocene. *Proceedings of the National Academy of Sciences of the United States of America*, *111*(43), 15296–15303. https://doi.org/10.1073/pnas.1411762111

Laskar, J., Robutel, P., Joutel, F., Gastineau, M., Correia, A. C. M., & Levrard, B. (2004). A long-term numerical solution for the insolation quantities of the Earth. *A&A*, *428*, 261–285. https://doi.org/10.1051/0004-6361:20041335

Leffingwell, E. D. K. (1915). Ground-ice wedges: The dominant form of ground-ice on the north coast of Alaska. *Journal of Geology*, *23*(7), 635–654. https://doi.org/10.1086/622281

Lisiecki, L. E., & Raymo, M. E. (2005). A Pliocene-Pleistocene stack of 57 globally distributed benthic δ^{18}O records. *Paleoceanography*, *20*, PA1003. https://doi.org/10.1029/2004pa001071

Lüthi, D., Le Floch, M., Bereiter, B., Blunier, T., Barnola, J.-M., Siegenthaler, U., et al. (2008). High-resolution carbon dioxide concentration record 650,000-800,000 years before present. *Nature*, *453*, 379–382. https://doi.org/10.1038/nature06949

Mackay, J. R., & Burn, C. R. (2002). The first 20 years (1978–1979 to 1998–1999) of ice-wedge growth at the Illisarvik experimental drained lake site, western Arctic coast, Canada. *Canadian Journal of Earth Sciences*, *39*, 95–111. https://doi.org/10.1139/e01-048

Manley, W. F., & Kaufman, D. S. (2002). *Alaska Paleo Glacier Atlas*. Institute of Arctic and Alpine Research (IN-STAAR), University of Colorado.

Meyer, H., Dereviagin, A., Siegert, C., Schirrmeister, L., & Hubberten, H.-W. (2002). Palaeoclimate reconstruction on Big Lyakhovsky Island, North Siberia – Hydrogen and oxygen isotopes in ice wedges. *Permafrost and Periglacial Processes*, *13*, 91–105. https://doi.org/10.1002/ppp.416

Meyer, H., Dereviagin, A. Y., Siegert, C., & Hubberten, H.-W. (2002). Paleoclimate studies on Bykovsky Peninsula, North Siberia – Hydrogen and oxygen isotopes in ground ice. *Polarforschung*, *70*, 37–51. https://doi.org/10.2312/polarforschung.70.37

Meyer, H., Opel, T., Laepple, T., Dereviagin, A. Y., Hoffmann, K., & Werner, M. (2015). Long-term winter warming trend in the Siberian Arctic during the mid- to late Holocene. *Nature Geoscience*, *8*, 122–125. https://doi.org/10.1038/ngeo2349

Meyer, H., Schirrmeister, L., Yoshikawa, K., Opel, T., Wetterich, S., Hubberten, H.-W., & Brown, J. (2010). Permafrost evidence for severe winter cooling during the Younger Dryas in northern Alaska. *Geophysical Research Letters*, *37*, L03501. https://doi.org/10.1029/2009gl041013

Meyer, H., Schönicke, L., Wand, U., Hubberten, H. W., & Friedrichsen, H. (2000). Isotope studies of hydrogen and oxygen in ground ice – Experiences with the equilibration technique. *Isotopes in Environmental and Health Studies*, *36*, 133–149. https://doi.org/10.1080/10256010008032939

Meyer, V. D., Hefter, J., Lohmann, G., Max, L., Tiedemann, R., & Mollenhauer, G. (2017). Summer temperature evolution on the Kamchatka Peninsula, Russian Far East, during the past 20 000 years. *Climate of the Past*, *13*, 359–377. https://doi.org/10.5194/cp-13-359-2017

Milankovitch, M. (1941). *Kanon der Erdbestrahlung und seine Anwendung auf das Eiszeitenproblem*. Royal Serbian Academy, Special Publication 133, Mathematics and Natural Sciences Section, Belgrade, 633 pp.

Murton, J. B., Goslar, T., Edwards, M. E., Bateman, M. D., Danilov, P. P., Savvinov, G. N., et al. (2015). Palaeoenvironmental interpretation of Yedoma silt (Ice Complex) deposition as cold-climate loess, Duvanny Yar, Northeast Siberia. *Permafrost and Periglacial Processes*, *26*, 208–288. https://doi.org/10.1002/ppp.1843

North Greenland Ice Core Project Members. (2004). High-resolution record of Northern Hemisphere climate extending into the last interglacial period. *Nature*, *431*, 147–151. https://doi.org/10.1038/nature02805

Opel, T., Dereviagin, A. Y., Meyer, H., Schirrmeister, L., & Wetterich, S. (2011). Palaeoclimatic information from stable water isotopes of Holocene ice wedges on the Dmitrii Laptev Strait, northeast Siberia, Russia. *Permafrost and Periglacial Processes*, *22*, 84–100. https://doi.org/10.1002/ppp.667

Opel, T., Laepple, T., Meyer, H., Dereviagin, A. Y., & Wetterich, S. (2017b). Northeast Siberian ice wedges confirm Arctic winter warming over the past two millennia. *The Holocene*, *27*, 1789–1796. https://doi.org/10.1177/0959683617702229

Opel, T., Meyer, H., Wetterich, S., Laepple, T., Dereviagin, A., & Murton, J. (2018). Ice wedges as archives of winter paleoclimate: A review. *Permafrost and Periglacial Processes*, *29*(3), 199–209. https://doi.org/10.1002/ppp.1980

Opel, T., Murton, J. B., Wetterich, S., Meyer, H., Ashastina, K., Günther, F., et al. (2019). Past climate and continentality inferred from ice wedges at Batagay megaslump in the Northern Hemisphere's most continental region, Yana Highlands, interior Yakutia. *Climate of the Past*, *15*, 1443–1461. https://doi.org/10.5194/cp-15-1443-2019

Opel, T., Wetterich, S., Meyer, H., Dereviagin, A. Y., Fuchs, M. C., & Schirrmeister, L. (2017a). Ground-ice stable isotopes and cryostratigraphy reflect late Quaternary palaeoclimate in the Northeast Siberian Arctic (Oyogos Yar coast, Dmitry Laptev Strait). *Climate of the Past*, *13*, 587–611. https://doi.org/10.5194/cp-13-587-2017

Petoukhov, V., Ganopolski, A., Brovkin, V., Claussen, M., Eliseev, A., Kubatzki, C., & Rahmstorf, S. (2000). CLIMBER-2: A climate system model of intermediate complexity. Part I: model description and performance for present climate. *Climate Dynamics*, *16*, 1–17. https://doi.org/10.1007/pl00007919

Porter, T. J., & Opel, T. (2020). Recent advances in paleoclimatological studies of Arctic wedge- and pore-ice stable-water isotope records. *Permafrost and Periglacial Processes*, *31*(3), 429–441. https://doi.org/10.1002/ppp.2052

Reimer, P. J., Austin, W. E. N., Bard, E., Bayliss, A., Blackwell, P. G., Bronk Ramsey, C., et al. (2020). The IntCal20 Northern Hemisphere radiocarbon age calibration curve (0-55 cal kBP). *Radiocarbon*, *62*(4), 725–757. https://doi.org/10.1017/rdc.2020.41

Rethemeyer, J., Gierga, M., Heinze, S., Stolz, A., Wotte, A., Wischhöfer, P., et al. (2019). Current sample preparation and analytical capabilities of the radiocarbon laboratory at CologneAMS. *Radiocarbon*, *61*(5), 1449–1460. https://doi.org/10.1017/rdc.2019.16

Schirrmeister, L., Kunitsky, V., Grosse, G., Wetterich, S., Meyer, H., Schwamborn, G., et al. (2011). Sedimentary characteristics and origin of the Late Pleistocene Ice Complex on north-east Siberian Arctic coastal lowlands and islands – A review. *Quaternary International*, *241*, 3–25. https://doi.org/10.1016/j.quaint.2010.04.004

Schirrmeister, L., Oezen, D., & Geyh, M. A. (2002). ^{230}Th/U dating of frozen peat, Bol'shoy Lyakhovsky Island (Northern Siberia). *Quaternary Research*, *57*, 253–258. https://doi.org/10.1006/qres.2001.2306

Spratt, R. M., & Lisiecki, L. E. (2016). A Late Pleistocene sea level stack. *Climate of the Past*, *12*, 1079–1092. https://doi.org/10.5194/cp-12-1079-2016

Svendsen, J., Alexanderson, H., Astakhov, V. I., Demidov, I., Dowdeswell, J. A., Funder, S., et al. (2004). Late quaternary ice sheet history of northern Eurasia. *Quaternary Science Reviews*, *23*, 1229–1271. https://doi.org/10.1016/j.quascirev.2003.12.008

Tierney, J. E., Zhu, J., King, J., Malevich, S. B., Hakim, G. J., & Poulsen, C. J. (2020). Glacial cooling and climate sensitivity revisited. *Nature*, *584*, 569–573. https://doi.org/10.1038/s41586-020-2617-x

Tumskoy, V. E. (2012). Osobennosti kriolitogeneza otlozhenii severnoi Yakutii v srednem Neopleistotsene-Golotsene [Peculiarities of cryolithogenesis in northern Yakutia from the Middle Neopleistocene to the Holocene]. *Kriosfera Zemli*, *16*, 12–21. (in Russian).

Vandenberghe, J., French, H. M., Gorbunov, A., Marchenko, S., Velichko, A. A., Jin, H., et al. (2014). The Last Permafrost Maximum (LPM) map of the Northern Hemisphere: permafrost extent and mean annual air temperatures, 25-17 ka BP. *Boreas*, *43*(3), 652–666. https://doi.org/10.1111/bor.12070

Weitzel, N., Hense, A., Herzschuh, U., Böhmer, T., Cao, X., & Rehfeld, K. (2021). A spatial reconstruction of Siberian Last Glacial Maximum climate from pollen data. *Climate Dynamics*. https://doi.org/10.31223/osf.io/76dfe

Wetterich, S., Kizyakov, A., Fritz, M., Wolter, J., Mollenhauer, G., Meyer, H., et al. (2020). The cryostratigraphy of the Yedoma cliff of Sobo-Sise Island (Lena delta) reveals permafrost dynamics in the central Laptev Sea coastal region during the last 52 kyr. *The Cryosphere*, *14*, 4525–4551. https://doi.org/10.5194/tc-14-4525-2020

Wetterich, S., Meyer, H., Opel, T., & Mollenhauer, G. (2021). Stable water isotope composition and radiocarbon dates of permafrost ice wedges from Bol'shoy Lyakhovsly Island (New Siberian Archipelago). *PANGAEA*. https://doi.pangaea.de/10.1594/PANGAEA.927621

Wetterich, S., Rudaya, N., Kuznetsov, V., Maksimov, F., Opel, T., Meyer, H., et al. (2019). Ice Complex formation on Bol'shoy Lyakhovsky Island (New Siberian Archipelago, East Siberian Arctic) since about 200 ka. *Quaternary Research*, *92*(2), 530–548. https://doi.org/10.1017/qua.2019.6

Wetterich, S., Rudaya, N., Tumskoy, V., Andreev, A. A., Opel, T., Schirrmeister, L., & Meyer, H. (2011). Last Glacial Maximum records in permafrost of the East Siberian Arctic. *Quaternary Science Reviews*, *30*, 3139–3151. https://doi.org/10.1016/j.quascirev.2011.07.020

Wetterich, S., Schirrmeister, L., Andreev, A. A., Pudenz, M., Plessen, B., Meyer, H., & Kunitsky, V. V. (2009). Eemian and Late Glacial/Holocene palaeoenvironmental records from permafrost sequences at the Dmitry Laptev Strait (NE Siberia, Russia). *Palaeogeography, Palaeoclimatology, Palaeoecology*, *279*, 73–95. https://doi.org/10.1016/j.palaeo.2009.05.002

Wetterich, S., Tumskoy, V., Rudaya, N., Andreev, A. A., Opel, T., Meyer, H., et al. (2014). Ice Complex formation in arctic East Siberia during the MIS3 Interstadial. *Quaternary Science Reviews*, *84*, 39–55. https://doi.org/10.1016/j.quascirev.2013.11.009

Wetterich, S., Tumskoy, V., Rudaya, N., Kuznetsov, V., Maksimov, F., Opel, T., et al. (2016). Ice Complex permafrost of MIS 5 age in the Dmitry Laptev Strait coastal region (East Siberian Arctic). *Quaternary Science Reviews*, *147*, 298–311. https://doi.org/10.1016/j.quascirev.2015.11.016

Willeit, M., & Ganopolski, A. (2015). Coupled Northern Hemisphere permafrost-ice-sheet evolution over the last glacial cycle. *Climate of the Past*, *11*, 1165–1180. https://doi.org/10.5194/cp-11-1165-2015

Reference From the Supporting Information

Stuiver, M., & Reimer, P. J. (1993). Extended ^{14}C data base and revised CALIB 3.0 ^{14}C age calibration program. *Radiocarbon*, *35*(1), 215–230. https://doi.org/10.1017/s0033822200013904